ACS OMEGA

http://pubs.acs.org/journal/acsodf

Article

Rare Silver–Histidine Cluster Complex and Its Single-Crystal-to-Single-Crystal Phase-Transition Behavior

Qingxin Liu, Yinglan Wu, Min Feng,* Wanmin Chen, and Zhiping Zheng*

Cite This: *ACS Omega* 2022, 7, 8141–8149

Read Online

ACCESS | Metrics & More | Article Recommendations | Supporting Information

ABSTRACT: Silver complexes with proteinogenic amino acid ligands are of interest for biomedical and antimicrobial applications. In this work, we obtained $\{[Ag_7(\text{L-his})_4](NO_3)_3{\cdot}3H_2O\}_{0.2}\{[Ag_8(\text{L-his})_4(H_2O)_2](NO_3)_4{\cdot}3H_2O\}_{0.8}$ (**1**) and $\{[Ag_7(\text{D-his})_4](NO_3)_3{\cdot}3H_2O\}_{0.2}\{[Ag_8(\text{D-his})_4(H_2O)_2](NO_3)_4{\cdot}3H_2O\}_{0.8}$ (**2**), which represent the first example of any Ag-exclusive complex featuring a cluster-type core motif and with only proteinogenic amino acid ligands. Upon immersion into acetonitrile, an interesting single-crystal-to-single-crystal transformation occurred to produce a new cluster complex of the formula $[Ag_8(\text{L-his})_4(NO_3)(H_2O)](NO_3)_3$ (**3**). Using a racemic mixture of histidine, the reaction under otherwise identical conditions led to the production of the second example of a three-dimensional (3D) network structured Ag-exclusive complex with only a proteinogenic amino acid ligand. Compared with other Ag–histidine complexes in the literature, the significance of reaction conditions, particularly the Ag/histidine ratio and pH of the reaction mixture, is revealed. Temperature-dependent emission of **1** and **2** at 440 nm characteristic of silver–philophilic interactions was also observed.

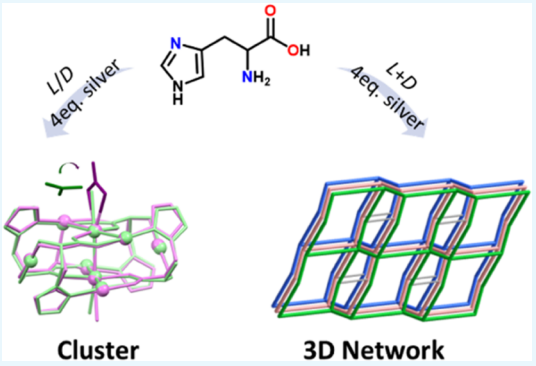

1. INTRODUCTION

Scientific exploration is frequently met with serendipitous discoveries. In our research of lanthanide clusters, which are a family of polynuclear lanthanide-containing complexes with aesthetically pleasing polyhedral core motifs and potential biomedical applications, small-unit anions such as halides are found to template their assembly from smaller and secondary building units.[1−8] For example, the cluster core of the wheel-like pentadecanuclear Nd(III) complex with L-histidine of the formula $[Nd_{15}(\mu_5\text{-Cl})(\mu_3\text{-OH})_{20}(\text{L-his})_{10}(\text{L-Hhis})_5(H_2O)_{10}]{\cdot}(ClO_4)_{14}$ (Figure 1a shows the cationic complex unit; Hhis, histidine; his, mono-deprotonated histidine) features five cubane-like $[Nd_4(\mu_3\text{-OH})_4]$ units centering around a μ_5-Cl (Figure 1b).[9] We treated this compound with $AgNO_3$ with the aim of obtaining the corresponding halide-free species, which would be an intriguing host for supramolecular chemistry of electron-rich guests or a powerful catalyst with multiple Lewis acidic sites.[10] Instant precipitation, presumably that of AgCl, was observed with the addition of $AgNO_3$. However, instead of the desirable halide-free wheel-like structure, we obtained a polynuclear Ag(I) complex whose structure was subsequently determined by single-crystal X-ray diffraction to be $\{[Ag_7(\text{L-his})_4](NO_3)_3{\cdot}3H_2O\}_{0.2}\{[Ag_8(\text{L-his})_4(H_2O)_2](NO_3)_4{\cdot}3H_2O\}_{0.8}$ (**1**). Nevertheless, this result is not entirely surprising as the wheel-like structure may not be adequately stable without the coordination of the five inner Nd(III) ions with μ_5-Cl. As such, the original Nd(III) cluster disassembled, releasing the histidine ligands that subsequently coordinate with $AgNO_3$ to produce **1**. This serendipitous polynuclear Ag–histidine complex appears to be quite unusual as it is, to the best of our knowledge, the first Ag-exclusive complex featuring a cluster-type core motif and with only proteinogenic amino acid ligands.

Many silver complexes display interesting photophysical properties,[11−21] and those of proteinogenic amino acid ligands are of particular interest due to their applications as antimicrobial agents[22−26] and for biosensing and drug delivery.[27] Stimulated by such useful applications and prompted by the unexpected production of **1**, we set out to prepare this new member of the Ag(I) complex family with the hope of directly synthesizing it by the reaction of L-histidine and $AgNO_3$ instead of going through the indirect and somewhat elusive procedure detailed above. Indeed, by controlling the pH condition of the reaction, we succeeded in the direct synthesis of **1** and its cognate $\{[Ag_7(\text{D-his})_4](NO_3)_3{\cdot}3H_2O\}_{0.2}\{[Ag_8(\text{D-his})_4(H_2O)_2](NO_3)_4{\cdot}3H_2O\}_{0.8}$ (**2**) using L- and D-histidine, respectively. We note that a number of differently structured Ag–histidine complexes have already been reported,[23,24,28,29] but they are either discrete mononuclear complex or one-dimensional polymeric

Received: January 6, 2022
Accepted: February 14, 2022
Published: February 23, 2022

https://doi.org/10.1021/acsomega.2c00094
ACS Omega 2022, 7, 8141–8149

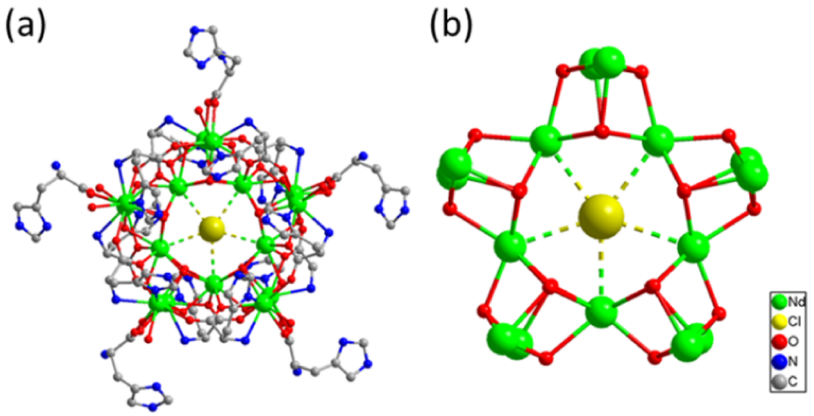

Figure 1. (a) Crystal structure of the cationic complex unit of $[Nd_{15}(\mu_5\text{-}Cl)(\mu_3\text{-}OH)_{20}(L\text{-his})_{10}(L\text{-Hhis})_5(H_2O)_{10}]^{14+}$ and (b) the structure of the inorganic core motif.[9]

chains wherein the histidine ligands display coordination modes that are quite different from in **1**. In this work, we detail the preparation and crystallographic structural analyses of **1** and **2**. Interestingly, we observed the single-crystal-to-single-crystal (SCSC) phase transition[30,31] of **1** to a new Ag(I) cluster complex of the formula $[Ag_8(L\text{-his})_4(NO_3)(H_2O)](NO_3)_3$ (**3**) upon immersion of **1** in acetonitrile. In addition, using a racemic mixture of L- and D-histidine under otherwise identical conditions, we obtained $[Ag_4(L\text{-his})(D\text{-his})(NO_3)_2]_n$ (**4**), which represents the very first Ag−histidine complex with a three-dimensional network structure, and the second example of a 3D network structure of any Ag-exclusive complex with only a proteinogenic amino acid ligand.[32]

2. EXPERIMENTAL SECTION

2.1. Materials and Methods. All reagents used throughout the study were of analytical grade, commercially available (from Macklin, Adamas, Shanghai Lingfeng, Aladdin), and used without further purifications. Deionized water with 18.3 MΩ (Merck Millipore) was used where applicable.

2.2. General Synthetic Procedures. *2.2.1. Synthesis of* $\{[Ag_7(L\text{-his})_4](NO_3)_3\cdot 3H_2O\}_{0.2}\{[Ag_8(L\text{-his})_4(H_2O)_2](NO_3)_4\cdot 3H_2O\}_{0.8}$ *(**1**).* $AgNO_3$ (340 mg, 2 mmol) and L-histidine (78 mg, 0.5 mmol) were dissolved in 7.5 mL of deionized water with stirring at 57 °C for about 5 min. To the above solution was added dropwise 0.5 M NaOH (ca. 450 μL) till an incipient but permanent precipitation was formed. The mixture was stirred for 1 h at 57 °C and then filtered. The filtrate at pH 5.5 was degassed with argon for 5 min, sealed, and allowed to stand at room temperature in the dark. Colorless plate-like crystals were obtained after 2 days with a yield of 10%. Elemental analysis calc.: C, 16.23; H, 2.34; N, 12.46%; found: C, 16.30; H, 2.23; N, 12.38%. Selected IR peaks (cm^{-1}): 3356br, 3305m, 3255m, 3134m, 1548s, 1300s, 1186m, 1080m, 818m, 634m.

2.2.2. Synthesis of $\{[Ag_7(D\text{-his})_4](NO_3)_3\cdot 3H_2O\}_{0.2}\{[Ag_8(D\text{-his})_4(H_2O)_2](NO_3)_4\cdot 3H_2O\}_{0.8}$ *(**2**).* Using D-histidine in place of L-histidine, compound **2** was obtained by adopting the same procedure used for the preparation of **1**. Colorless plate-like crystals were obtained with a yield of 10%. Elemental analysis calc.: C, 16.23; H, 2.34; N, 12.46%; found: C, 16.28; H, 2.20; N, 12.36%. Selected IR peaks (cm^{-1}): 3367br, 3321m, 3257m, 3136m, 1552s, 1304s, 1186m, 1076m, 823m, 633m.

*2.2.3. Transformation of **1** to* $[Ag_8(L\text{-his})_4(NO_3)(H_2O)](NO_3)_3$ *(**3**).* Single crystals (5 mg) of **1** were placed in a 3 mL vial with 1 mL of CH_3CN at room temperature. The sample recovered after 15 days suffered from severe cracking, but the uncracked fragments remained crystalline and were suitable for single-crystal X-ray diffraction studies. Selected IR peaks (cm^{-1}): 3309m, 3259m, 3116m, 1550s, 1308s, 1192m, 1068m, 818m, 633m.

2.2.4. Synthesis of $[Ag_4(L\text{-his})(D\text{-his})(NO_3)_2]_n$ *(**4**).* This compound was prepared by adopting the same procedure used for the synthesis of **1** with a racemic mixture of L- and D-histidine in place of L-histidine. The product was obtained as colorless plate-like crystals (yield of 10%). Elemental analysis calc.: C, 16.69; H, 1.87; N, 12.97%; found: C, 16.76; H, 1.60; N, 12.86%. Selected IR peaks (cm^{-1}): 3319m, 3257m, 3128m, 1558s, 1327s, 1138m, 1157m, 937m, 818m, 768m, 625m.

2.3. X-ray Diffraction Analysis. *2.3.1. Single-Crystal X-ray Diffraction.* Single-crystal X-ray diffraction data were collected on a Bruker D8 Venture diffractometer using graphite monochromatized Mo Kα radiation (λ= 0.71073 Å) at 100 K. Data collection and reduction were performed using the program APEX3. Absorption corrections were applied using the multiscan program SADABS. The structures were solved by the intrinsic phasing method (SHELXT)[33] and using Olex2[34] as the graphical interface, and the nonhydrogen atoms were refined anisotropically by a full-matrix least-squares method on F^2. All nonhydrogen atoms in the complexes are corrected for anisotropy. The nonhydrogen atoms are hydrogenated according to the theoretical background of structural chemistry, and the hydrogen atoms are further fixed on the carbon atoms. Crystal data, data collection parameters, and details of the structure refinement are given in Table S1. Selected bond lengths and bond angles are listed in Tables S2−S7. More than 10 measurements were performed to confirm the disorder ratio of **1**.

2.3.2. Powder X-ray Diffraction. PXRD patterns were obtained on a Rigaku Smartlab X-ray diffractometer using Cu Kα radiation (λ = 1.54178 Å). The voltage and the current were 40 kV and 100 mA, respectively. The samples were measured in reflection mode in the 2θ range of 5−50° with a scan speed of 10° min^{-1}. All of the data were acquired at ambient temperature.

2.4. Thermal Analysis. Thermogravimetric analyses of samples were manipulated for thermal stability using a METTLER TOLEDO TGA2 instrument. The measurements were carried out with 2−5 mg samples at a rate of 10 °C min^{-1} from 30 to 800 °C under argon protection.

https://doi.org/10.1021/acsomega.2c00094
ACS Omega 2022, 7, 8141−8149

Table 1. Silver−Histidine Coordination Compounds with Crystal Structures and Their Synthetic Conditions

formula	Ag/L[a]	pH	silver source	chirality	histidine type	Ag/L[b]	structure	ref
$[(\{Ag(L\text{-}H_2his)(NO_3)_2\}_2)H_2O]_n$	1:1	3−4[c]	$AgNO_3$	chiral	H_2his^+	1:1	1D chain	29
$[Ag_2(L\text{-}H_2his)(D\text{-}H_2his)(NO_3)_4]_n$	1:1	3−4[c]	$AgNO_3$	racemic	H_2his^+	1:1	1D chain	29
$[\{Ag(D/L\text{-}Hhis)_2NO_3\}_2]\cdot H_2O$	1:1	5.0−5.5[d,f]	$AgNO_3$	chiral	$Hhis^0$	1:2	mononuclear	29
$[Ag_2(D\text{-}his)(L\text{-}his)]_n$	1:2	ca. 7.5[d,f]	Ag_2O	racemic	his^-	1:1	1D chain	24
$[Ag(D/L\text{-}his)]_n$	1:2	ca. 8[d,f]	Ag_2O	chiral	his^-	1:1	1D chain	23, 24
$\{[Ag_7(L\text{-}his)_4](NO_3)_3\cdot 3H_2O\}_{0.2}$ $\{[Ag_8(L\text{-}his)_4(H_2O)_2](NO_3)_4\cdot 3H_2O\}_{0.8}$	4:1	ca. 5.5[e]	$AgNO_3$	chiral	his^-	7.8:4	multinuclear clusters	this work
$[Ag_4(L\text{-}his)(D\text{-}his)(NO_3)_2]_n$	4:1	ca. 5.5[e]	$AgNO_3$	racemic	his^-	2:1	3D network	this work

[a]Reactant ratio. [b]Composition ratio. [c]HNO_3 was added. [d]Neither base nor acid was added, pH not mentioned. [e]NaOH was added. [f]pH value from our reproduction of the literature experiments.

2.5. FT-IR Spectroscopy. Fourier transform infrared (FT-IR) spectra were collected on a Bruker Vertex80 FT-IR spectrometer via the attenuated total reflection method (ATR) in the range of 4000−600 cm^{-1}.

2.6. pH Measurement. pH values in this work were estimated using commercial special pH test strips (Shanghai SSS, range: 6.4−8.0, 5.5−9.0, 3.8−5.4). For comparison with the Ag−histidine complexes in the literature, we reproduced the solution mixtures according to the reported procedure and measured their pH values. The results are collected in Table 1.

2.7. Photophysical Measurements. Luminescence measurements were performed on an Edinburgh Instruments FLS1000 photoluminescence spectrometer. Absorption spectra were recorded using an Agilent Technologies Cary 5000 UV−vis−NIR spectrophotometer equipped with an integration sphere.

3. RESULTS AND DISCUSSION

3.1. Synthesis. We conducted a thorough literature survey to find the Ag−histidine complexes collected in Table 1. It is clear that the identity of the complexes is sensitively dependent on the Ag(I) source, the Ag/histidine ratio, the optical purity (optical pure D- or L-histidine, or a racemic mixture) of the ligand, and the pH of the reaction mixture. Quite different from the literature work, our synthesis used a much higher Ag/histidine ratio; the excess amount of Ag(I) served as an indicator when the original reaction mixture was "titrated" with a freshly prepared NaOH solution. The formation of incipient but permanent precipitation indicated the complete coordination of any deprotonated histidine ligand with Ag(I); any further addition of NaOH would lead to the precipitation of AgOH. Our synthesis thus represents a distinct preparative paradigm in that all of the potential coordinating atoms of the histidine ligands are fully utilized because of the complete ligand deprotonation of the carboxylic acid by NaOH.

The enantiomeric **2** was synthesized in the same manner as **1** with D-histidine. Interestingly, when **1** is immersed in acetonitrile, compound **3** is obtained via SCSC transformation with the loss of an axially bound aqua ligand. The 3D network **4** is obtained under the same reaction condition as **1** and **2** with the racemic histidine ligand.

3.2. Crystallographic Studies. *3.2.1. Structure of* $\{[Ag_7(his)_4](NO_3)_3\cdot 3H_2O\}_{0.2}\{[Ag_8(his)_4(H_2O)_2](NO_3)_4\cdot 3H_2O\}_{0.8}$ *(**1**, **2**).* The enantiomeric **1** and **2** are crystallized in the chiral orthorhombic space group $C222_1$ (no. 20) with negligible Flack parameters of −0.012(9) and 0.022(15), respectively, indicating their homochirality (Table S1). As **1** and **2** (Figure S1) are enantiomeric, only the structure of **1** is discussed below.

The asymmetric unit is composed of half of the molecule of **1** due to a C_2 axis along the *b*-axis (Figure 2). Two disordered

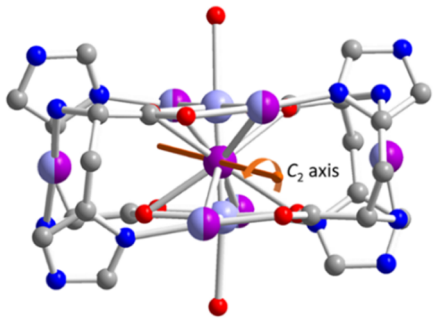

Figure 2. Ball-and-stick model of the "mixture" structure of **1** with Ag_7 and Ag_8 substructures. Hydrogen atoms, counter anions, and free solvent molecules of crystallization are omitted for clarity. Color code: purple, Ag atoms in Ag_7 substructure; pale blue, Ag atoms in Ag_8 substructure; red, O; blue, N; and gray, C.

complex units are found with a statistical overlaying of $[Ag_7(his)_4](NO_3)_3$ (an Ag_7 substructure) at 20% and $[Ag_8(his)_4(H_2O)_2](NO_3)_4$ (an Ag_8 substructure) at 80%. This crystallographic disorder shows consistent reproducibility in more than 10 different batches of samples. All Ag atoms and the organic ligands are Ag(I) and mono-deprotonated as L-his, respectively. Selected bond lengths and angles are collected in Tables S2 and S3.

The cationic Ag_7 substructure (Figure 3a) consists of an Ag_5 core (Ag1B, Ag2, Ag2′, Ag3, Ag3′), two flanking Ag ions (Ag4, Ag4′) with one on each side of the Ag_5 core, and four L-his ligands. The central Ag_5 motif, featuring Ag···Ag interactions between adjacent Ag atoms, can be viewed as two staggered corner-sharing isosceles triangles with a dihedral angle of 58.078(6)° and a C_2 axis passing through the central Ag1B and bisecting the two triangles. The Ag···Ag separations ranging from 2.9053(9) to 3.333(3) Å (Table S2) are less than twice the van der Waals radius of Ag(I) at 3.44 Å but more than twice the silver radius of 2.88 Å.[35−37] Silver−philophilic interactions are thus established. The Ag(I) ions are situated in three different coordination environments. Specifically, in addition to interacting Ag2, Ag2′, Ag3, and Ag3′, the central Ag1B is coordinated with four carboxylate O atoms (O2, O2′, O3, O3′) from four different L-his ligands, forming a compressed tetrahedral coordination geometry with an average Ag−O bond length of 2.5255 Å. For the other Ag atoms in the

https://doi.org/10.1021/acsomega.2c00094
ACS Omega 2022, 7, 8141−8149

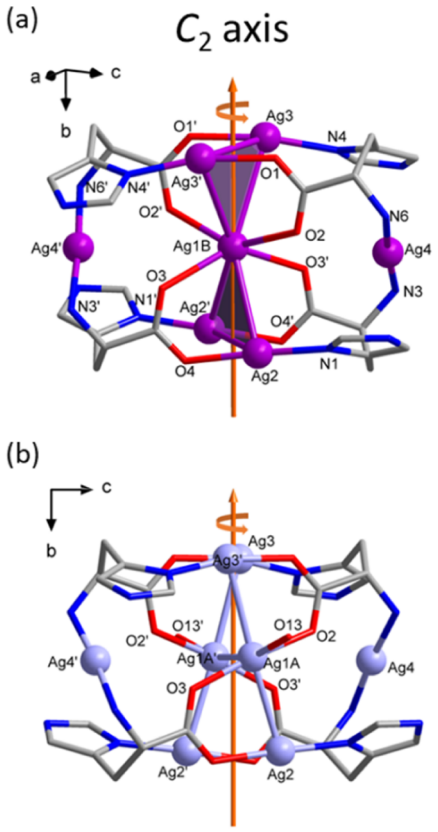

Figure 3. (a, b) Ag_7 and Ag_8 substructures of **1**, respectively. Hydrogen atoms, counter anions, and free solvent molecules of crystallization are omitted for clarity. Color code: purple (a), pale blue (b), Ag; red, O; blue, N; and gray, C.

core motif, namely, Ag2, Ag2′, Ag3, and Ag3′, a similar coordination environment is observed: each of the Ag atoms is coordinated linearly with one carboxylate O and one amino N atom from two different L-his ligands with an average N−Ag−O angle of 171.65° and average Ag−O and Ag−N bond lengths of 2.1335 and 2.1185 Å, respectively. In comparison, the two peripheral Ag atoms (Ag4, Ag4′), aligned linearly with the central Ag1B, are each coordinated with two amino N atoms from two different L-his ligands with an N−Ag−N angle of 175.5(2)° and an average Ag−N bond length of 2.165 Å. All L-his ligands display the same μ_4:η^1,η^1,η^1,η^1 coordination mode with all four coordinating atoms utilized. The number of occupied coordination sites of the ligands in **1** is higher than that in the previously reported Ag−histidine complexes (Table 1); this higher degree of utilization of the coordinating atoms is responsible for the formation of the more sophisticated structures in the present work.

The cationic Ag_8 substructure is shown in Figure 3b. The most noticeable difference compared with the Ag_7 substructure is the replacement of the central Ag1B in Ag_7 by two Ag(I) ions (Ag1A and Ag1A′), resulting in a distorted "H"-shaped arrangement of the central motif with torsion angles of 34.455(24) and 30.040(24)° for Ag2−Ag1A−Ag1A′−Ag2′ and Ag3′−Ag1A−Ag1A′−Ag3, respectively. The Ag···Ag distances in this Ag_6 arrangement, ranging from 2.9053(9) to 3.2843(13) Å, also fall in the expected range for silver−philophilic interactions.[35−37] A C_2 axis also exists in the structure, passing through the midpoint of the "H" rung (Ag1A−Ag1A′). The two sides of "H" (Ag3−Ag1A′−Ag2′ and Ag3′−Ag1A−Ag2) are essentially linear with an angle of 177.75 (3)°. They are almost perpendicular to the rung with angles of 90.784 (19) and 89.67(2)° for Ag2−Ag1A−Ag1A′ and Ag3′−Ag1A−Ag1A′, respectively. In addition to the Ag··· Ag interactions, the central Ag1A is coordinated with three O atoms, two carboxylato O atoms (O2, O3) from two different L-his ligands with an average Ag−O bond length of 2.1255 Å, and one aqua O atom (O13) with the Ag−O bond length at 2.466(14) Å.

*3.2.2. SCSC Phase Transition from **1** to **3**.* Single crystals of **1** were transformed into single crystals of compound **3** with the formula $[Ag_8(L\text{-his})_4\ (NO_3)(H_2O)](NO_3)_3$ after immersion in acetonitrile for 15 days. The newly formed **3** crystallized in the chiral monoclinic space group $P2_1$ (no. 4), and its structure is shown in Figure 4.

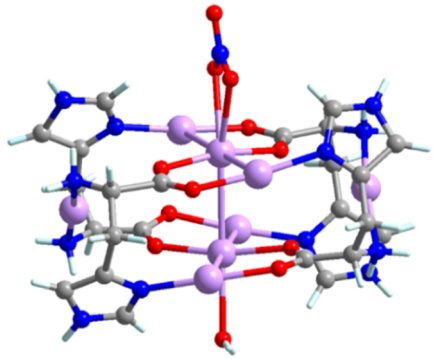

Figure 4. Crystal structure of **3**, with counter anions omitted for clarity. Color code: mauve, Ag; red, O; blue, N; and gray, C; turquoise, H.

The overlay of the structure of **3** and that of the Ag_8 substructure of precursor **1** reveals a striking similarity between their overall architectures (Figure 5). However, the following

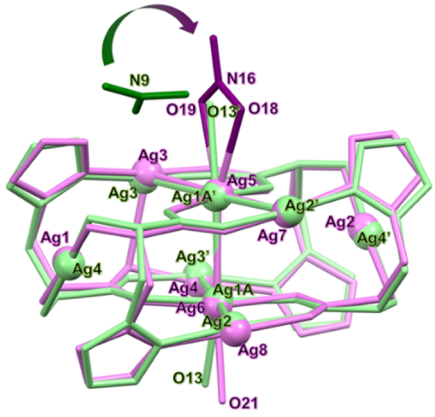

Figure 5. Overlay of **3** and Ag_8 substructure of **1**: green, Ag_8 substructure of **1**; and pink, **3**. All metal atoms are overlain. Hydrogen atoms, counter anions, and free solvent molecules of crystallization are omitted for clarity.

significant differences could be noticed. The C_2 axis in **1** is lost in **3** as its rung Ag atoms (Ag5 and Ag6) are no longer crystallographically equivalent, resulting from one of the aqua ligands in **1** (O13′ coordinated to Ag1A′) being substituted by a nitrato ligand (O18 and O19 of the nitrato coordinated to Ag5) in a chelating η^2 fashion (Figure 5). The remaining aqua

https://doi.org/10.1021/acsomega.2c00094
ACS Omega 2022, 7, 8141−8149

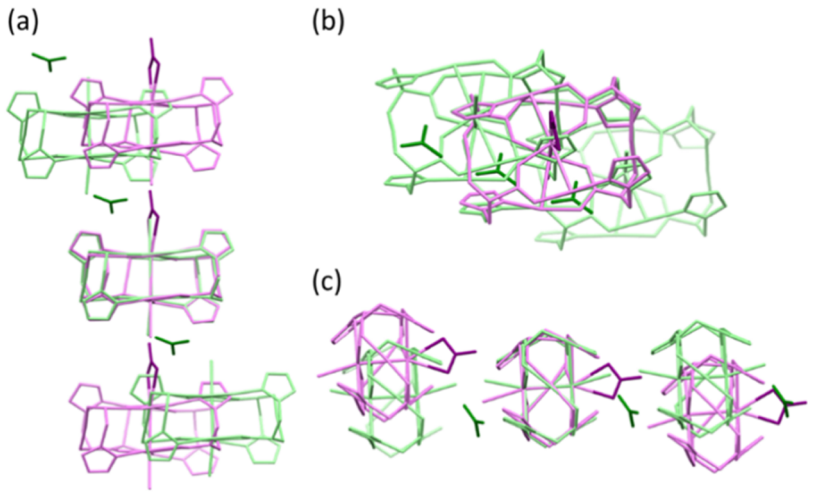

Figure 6. Comparison of the crystal packing of **3** (pink) and Ag_8 substructure of **1** (green) along three different directions (a–c). Hydrogen atoms, counter anions, and free solvent molecules are omitted for clarity.

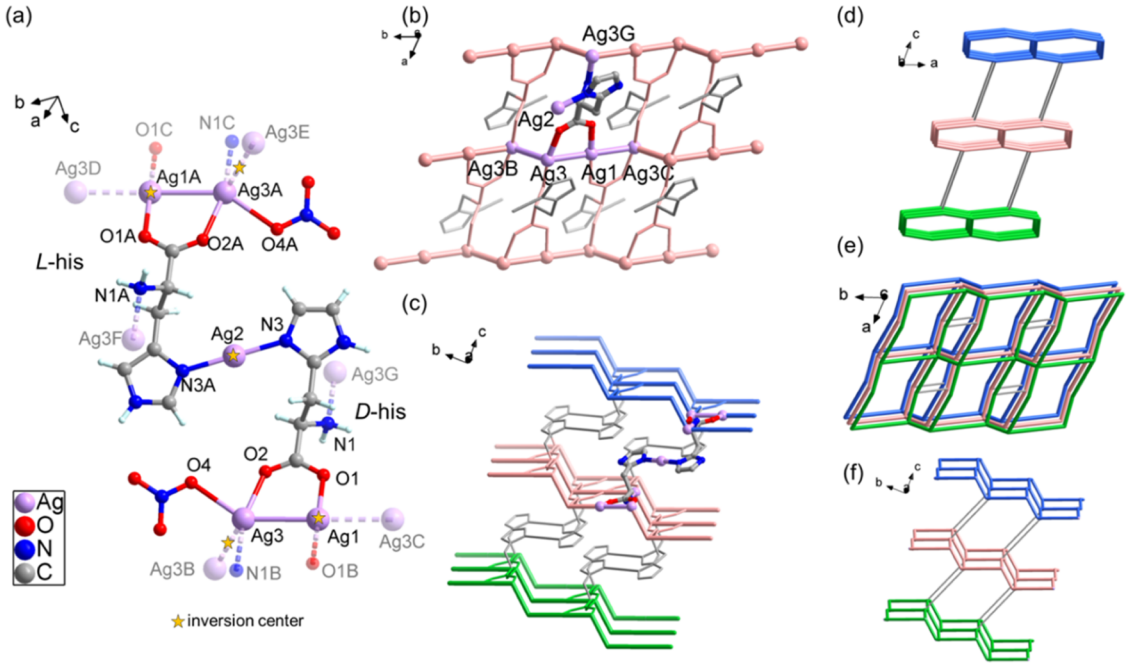

Figure 7. (a) Repeating unit Ag_4(L-his)(D-his)$(NO_3)_2$ in **4**, extended atoms are translucent; (b) 2D network of **4**, hydrogen and nitrate atoms are omitted for clarity; (c) 3D network of **4**, hydrogen and nitrate atoms are omitted for clarity; and (d–f) topology of the 3D structure, viewed from different directions.

ligand (O21 on Ag6) is slightly off position with respect to the corresponding coordination (O13 on Ag1A) in **1**. It is also of note that there are no water molecules of crystallization like in **1**, which may have induced the change in crystal packing in three directions as illustrated in Figure 6. As such, sufficient stress may have been built up, leading to the cracking of the crystals of **3** during the SCSC transformation from **1**. The loss of water molecules, which might be caused by the acetonitrile, is also verified by IR measurements; the O–H stretching vibration of water around 3200 cm^{-1} in **1** diminishes in **3** (Figure S8). Selected bond lengths and angles of **3** are summarized in Tables S4 and S5. Different solvents were also tested for the SCSC transformation, with the resulting PXRD patterns (Figure S6) showing that this SCSC transformation might be solvent dependent.

*3.2.3. Structure of $[Ag_4$(L-his)(D-his)$(NO_3)_2]_n$ (**4**).* The racemic 3D coordination network **4** crystallized in the triclinic space group *P*-1 (no. 2). An asymmetric unit consists of one Ag(I) ion (Ag3), two half Ag(I) ions (Ag1 and Ag2), one his, and one NO_3^-. The crystallographic occupancies are 1 for Ag3 and 0.5 for Ag1 and Ag2. Two asymmetric units form a repeating unit of Ag_4(L-his)(D-his)$(NO_3)_2$ for the polymeric structure (Figure 7a). Ag1 is coordinated linearly with two carboxylato O (O1, O1B), one from an L-his and the other from a D-his ligand as required by the inversion center located at Ag1. Ag2 is coordinated linearly with two imidazolo N (N3, N3A) from two different his ligands of opposite chiralities due to the other inversion center located at Ag2. Ag3 is in a NO_2 coordination environment with an O (O4) of a monodentate nitrato ligand, one carboxylato O (O2), and one amino N

https://doi.org/10.1021/acsomega.2c00094
ACS Omega 2022, 7, 8141–8149

(N1B) atoms from two different his ligands of the same chirality. The Ag−O bond lengths range from 2.142(4) to 2.544(5) Å, while the Ag−N bond lengths range from 2.064(7) to 2.232(5) Å. Selected bond lengths and angles are collected in Tables S6 and S7.

The Ag···Ag distance of Ag1−Ag3 (2.9076(7) Å) and that between neighboring Ag3 ions (3.0411(10) Å) fall in the range for silver−philophilic interactions.[35−37] The inversion center at Ag1 leads to a linear Ag3−Ag1−Ag3C arrangement. Moreover, the inversion center between two adjacent Ag3 ions results in an infinite stair-like silver−philophilic chain along *b*-axis with the trimeric Ag units serving as secondary building units. These chains are linked by his ligands whose carboxylate group bridges two Ag(I) ions (Ag3, Ag1) on one chain, while its amino group links one Ag(I) ion (Ag3G) on the other chain, forming a 2D network (Figure 7b). The his imidazole groups lie between the 2D networks are linked by Ag2, leading to the formation of a 3D network (Figure 7c), which has a 3,4-connected 2-nodal net topology (jeb, bbe-3,4-Cmmm) with the point symbol of $\{6^3\}\{6^5.8\}$ (Figure 7d−f).

3.3. Powder X-ray Diffraction Analyses and Thermal Analyses. The phase purities of **1**−**4** are confirmed by PXRD measurements (Figures S3−S7). From the TGA profile (Figure S9), the weight loss at around 100 °C correspond to the loss of the free water (**1**: obsd: 2.57%, calcd: 3.04%; **2**: obsd: 2.73%, calcd: 3.04%; **4**: obsd: 0.17%, calcd: 0%). The weight loss stages at ∼200 °C reveal the skeletons of four complexes are stable until 200 °C.

3.4. Comparisons of Ag−Histidine Complexes. All Ag−histidine complexes with a crystal structure are collected in Table 1. As can be seen, the determining reaction variables for synthesizing these complexes include pH (3−8), silver source ($AgNO_3$ or Ag_2O), reactant ratio (Ag/histidine from 1:2 to 4:1), and optical purity of the ligand (chiral or racemic). Different pH conditions can be achieved with the addition of an acid, a base, or nothing at all to generate various forms of histidine with different degrees of protonation or deprotonation.

As shown in Figure 8, these forms of histidine offer two, three, or four coordinating atoms. Accordingly, in the reported

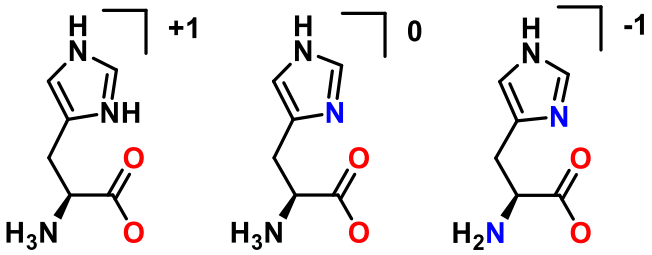

Figure 8. Potential coordination sites (in color) of three different forms of histidine.

Ag−H_2his$^+$ 1D chains, two coordination sites of H_2his$^+$ are occupied by two Ag(I) ions (Figure S10a).[29] However, in the reported Ag−Hhis^0 mononuclear complex[29] and Ag−his 1D chains,[23,24] only one, two, and three coordination sites are occupied, respectively (Figure S10b,c). In other words, the available coordination sites are not completely used, probably due to insufficient Ag because of the small Ag:histidine ratio (1:2 to 1:1); only mononuclear complex and 1D chain complex were obtained regardless of the optical purity of the ligand used.

In addition to the number of coordination sites in histidine ligand, flexibility plays a vital role in the diversity of the structures. The rotation of the *αβ*-C−C bond offers two patterns of histidine ligand: convergent (Figure 9a) and

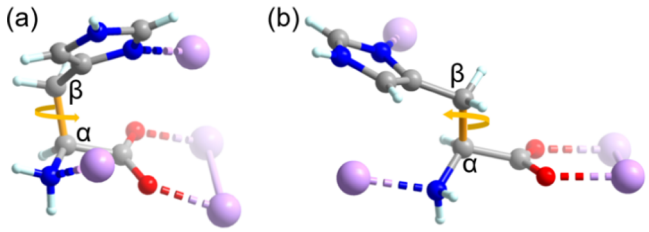

Figure 9. *αβ*-C−C bond rotation and coordination modes in **1** (a) and **4** (b). Color code: mauve, Ag; red, O; blue, N; gray, C; and turquoise, H.

divergent (Figure 9b). In the previously reported Ag−histidine structures, the convergent modes are found in Ag−H_2his$^+$ and Ag−Hhis^0 complexes (Figure S10a,b),[29] while the divergent mode are found in Ag−his complexes (Figure S10c).[23,24]

In stark contrast, we obtain the his ligand with four coordination sites by deprotonating the ligand with NaOH. Furthermore, the Ag:histidine ratio was increased to 4:1 to ensure the complete utilization of all four coordinating atoms. In Figure 9a, the his ligand shows a convergent coordination configuration, which is propitious to the formation of a discrete and closed cluster structure (**1** and **2**) by connecting a finite number of Ag atoms. In stark contrast, acting as a bridge, the his stretches out to link a number of Ag atoms in a divergent fashion (Figure 9b), resulting in the formation of the three-dimensional network structure.

3.5. Photoluminescence Properties. The photoluminescence properties of **1** and **2** were analyzed in the solid state with both showing similar optical behaviors (Figures 10 and S15−S19). Upon irradiation at 290 nm in the histidine-centered absorption band (Figure S14), a blue emission of **1** with Commission Internationale de l'Éclairage (CIE) coordinates of (0.19, 0.16) (Figure S12) centered at 440 nm was observed at 78 K (Figure 10a). To investigate the relationship between luminescence intensity and temperature, the emission spectra of **1** and **2** in the solid state were monitored, showing that the emission intensity is highly sensitive to temperatures (Figure S10b) and excitation energies (Figure S11). As shown in Figure 10b, when the temperature is increased from 78 to 198K, the emission intensity of **1** dramatically decreases, which may be rationalized in terms of the shorter Ag−Ag contacts at a lower temperature as a result of a more rigid cluster structure and stronger silver−philophilic interactions.[36,38] Lifetime decay profile of **1** fitted by a biexponential function showed a lifetime of 50 *μ*s at 78 K, and this value at the microsecond scale suggests phosphorescence.[39] However, the three-dimensional network **4** was found to be nonemissive. Despite the many common structural features shared by **1**, **2**, and **4** (the same ligand coordination mode and his/Ag ratio and similar Ag···Ag distances), a more detailed structural comparison showed that the Ag atoms in the chain of **4** are less engaged in silver−philophilic interactions. Specifically, there are only two Ag···Ag interactions involving Ag1 and Ag3 in **4**, while four such interactions are found in **1** and **2** between Ag1B and Ag2, Ag2′, Ag3, and Ag3′ (Figure 3). Therefore, the luminescence of **1** and **2** might be attributed to their cluster structural characteristics with more silver−philophilic interactions for

https://doi.org/10.1021/acsomega.2c00094
ACS Omega 2022, 7, 8141−8149

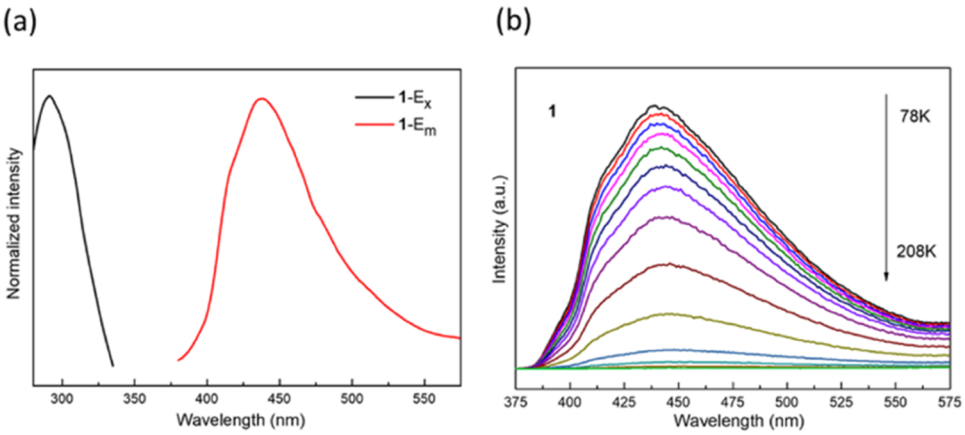

Figure 10. (a) Solid-state excitation (λ_{em} = 440 nm, black line) and emission spectra (λ_{ex} = 290 nm, red line) of **1** at 78 K. (b) Temperature-dependent luminescence spectra of **1** (λ_{ex} = 290 nm) from 78 to 208 K.

each Ag atom, while such interactions are not extensive enough for the 3D network **4** to be emissive under the same excitation conditions.

4. CONCLUSIONS

In this work, using either optically pure L- or D-histidine as ligand and carefully controlling the Ag/histidine ratio as well as the pH condition of the reaction mixture, we succeeded in synthesizing three new Ag−histidine complexes, two of which were enantiomeric and emissive, possessing a discrete cluster-type of structure with an Ag_7/Ag_8 core motif linked and encapsulated by histidine ligands (**1**, **2**), which were the first Ag-exclusive clusters with only proteinogenic amino acid ligands. Upon immersion of one of these crystals in acetonitrile, single-crystal-to-single-crystal transformation occurred to produce yet another new Ag8 cluster complex with histidine (**3**). Using a racemic mixture of histidine, the reaction under otherwise identical conditions led to the production of the very first Ag-exclusive histidine complex with a 3D network structure (**4**), which was also only the second one of any Ag-exclusive complexes with only a proteinogenic amino acid ligand. It was the meticulous adjustment of the reaction conditions that led to the unique coordination mode of the ligands and the resulting uniquely structured complexes. The new preparation methods and the diverse coordination modes displayed by the new Ag−histidine complexes presented in this work may stimulate more future research to further the chemistry of Ag−amino acid complexes that is driven primarily by their biomedical and antimicrobial applications.

■ ASSOCIATED CONTENT

Supporting Information

The Supporting Information is available free of charge at https://pubs.acs.org/doi/10.1021/acsomega.2c00094.

Discussions of tables of crystallographic data and structural refinement parameters, selected bond distances and bond angles, figures of the structure of **2**, coordination modes, PXRD patterns, TGA, IR curves, photographs of crystals, solid-state excitation, emission, and absorption spectra, emission decay curve, and CIE chromaticity diagram (PDF)

Accession Codes

Accession Codes CCDC 2131102, 2128164, 2128457, and 2128456 contain the supplementary crystallographic data for this paper. These data can be obtained free of charge via www.ccdc.cam.ac.uk/data_request/cif, or by emailing data request@ccdc.cam.ac.uk, or by contacting The Cambridge Crystallographic Data.

■ AUTHOR INFORMATION

Corresponding Authors

Min Feng − *Department of Chemistry, Southern University of Science and Technology, Shenzhen 518055, China*; Email: fengm@sustech.edu.cn

Zhiping Zheng − *Department of Chemistry, Southern University of Science and Technology, Shenzhen 518055, China; Department of Chemistry and Biochemistry, The University of Arizona, Tucson, Arizona 85721, United States*; orcid.org/0000-0002-5834-6763; Email: zhengzp@sustech.edu.cn

Authors

Qingxin Liu − *Department of Chemistry, Southern University of Science and Technology, Shenzhen 518055, China*

Yinglan Wu − *Department of Chemistry and Biochemistry, The University of Arizona, Tucson, Arizona 85721, United States*

Wanmin Chen − *Department of Chemistry, Southern University of Science and Technology, Shenzhen 518055, China*

Complete contact information is available at: https://pubs.acs.org/10.1021/acsomega.2c00094

Notes

The authors declare no competing financial interest.

■ ACKNOWLEDGMENTS

This work was financially supported by the National Natural Science Foundation of China (Grant No. 21971106), the Shenzhen Nobel Prize Scientists Laboratory Project (Grant No. C17783101), the Stable Support Project of Key Research Plan of Shenzhen , startup fund from SUSTech (Grant Nos. Y01216127, Y01216227), Shenzhen Postdoctoral Research Fund (Grant Nos. K21217521, K21217512), the Stable Support Plan Program of Shenzhen Natural Science Fund (Grant No. 20200925161141006), and Guangdong Basic and Applied Basic Research Foundation (Grant No. 2021A1515110855).

ABBREVIATIONS

his, mono-deprotonated histidine; SCSC, single crystal to single crystal; CIE, Commission Internationale de l'Éclairage

REFERENCES

(1) Kong, X.-J.; Wu, Y.; Long, L.-S.; Zheng, L.-S.; Zheng, Z. A Chiral 60-Metal Sodalite Cage Featuring 24 Vertex-Sharing $[Er_4(\mu_3\text{-}OH)_4]$ Cubanes. *J. Am. Chem. Soc.* **2009**, *131*, 6918−6919.

(2) Kong, X.-J.; Ren, Y.-P.; Chen, W.-X.; Long, L.-S.; Zheng, Z.; Huang, R.-B.; Zheng, L.-S. A Four-Shell, Nesting Doll-like 3d−4f Cluster Containing 108 Metal Ions. *Angew. Chem., Int. Ed.* **2008**, *47*, 2398−2401.

(3) Zheng, X.-Y.; Kong, X.-J.; Zheng, Z.; Long, L.-S.; Zheng, L.-S. High-Nuclearity Lanthanide-Containing Clusters as Potential Molecular Magnetic Coolers. *Acc. Chem. Res.* **2018**, *51*, 517−525.

(4) Bao, G.; Wen, S.; Lin, G.; Yuan, J.; Lin, J.; Wong, K.-L.; Bünzli, J.-C. G.; Jin, D. Learning from lanthanide complexes: The development of dye-lanthanide nanoparticles and their biomedical applications. *Coord. Chem. Rev.* **2021**, *429*, No. 213642.

(5) Zheng, Z. Ligand-controlled self-assembly of polynuclear lanthanide−oxo/hydroxo complexes: from synthetic serendipity to rational supramolecular design. *Chem. Commun.* **2001**, 2521−2529.

(6) Zheng, X.-Y.; Xie, J.; Kong, X.-J.; Long, L.-S.; Zheng, L.-S. Recent advances in the assembly of high-nuclearity lanthanide clusters. *Coord. Chem. Rev.* **2019**, *378*, 222−236.

(7) Li, X.-Y.; Jing, Y.; Zheng, J.; Ding, H.; Li, Q.; Yu, M.-H.; Bu, X.-H. Two Luminescent High-Nuclearity Lanthanide Clusters Ln_{48} (Ln = Eu and Tb) with a Nanopillar Structure. *Cryst. Growth Des.* **2020**, *20*, 5294−5301.

(8) Su, Y.-M.; Ji, B.-Q.; Wang, Z.; Zhang, S.-S.; Feng, L.; Gao, Z.-Y.; Li, Y.-W.; Tung, C.-H.; Sun, D.; Zheng, L.-S. Anionic passivation layer-assisted trapping of an icosahedral Ag_{13} kernel in a truncated tetrahedral Ag_{89} nanocluster. *Sci. China Chem.* **2021**, *64*, 1482−1486.

(9) Huang, W.; Zhang, Z.; Wu, Y.; Chen, W.; Rotsch, D. A.; Messerle, L.; Zheng, Z. A systematic study of halide-template effects in the assembly of lanthanide hydroxide cluster complexes with histidine. *Inorg. Chem. Front.* **2021**, *8*, 26−34.

(10) Huang, W.; Liu, Q.; Chen, W.; Feng, M.; Zheng, Z. Recent Advances in the Catalytic Applications of Lanthanide-Oxo Clusters. *Magnetochemistry* **2021**, *7*, 161.

(11) Li, S.; Yan, Z.-P.; Li, X.-L.; Kong, Y.-J.; Li, H.-Y.; Gao, G.-G.; Zheng, Y.-X.; Zang, S.-Q. Stepwise Achievement of Circularly Polarized Luminescence on Atomically Precise Silver Clusters. *Adv. Sci.* **2020**, *7*, No. 2000738.

(12) Li, S.; Du, X.-S.; Li, B.; Wang, J.-Y.; Li, G.-P.; Gao, G.-G.; Zang, S.-Q. Atom-Precise Modification of Silver(I) Thiolate Cluster by Shell Ligand Substitution: A New Approach to Generation of Cluster Functionality and Chirality. *J. Am. Chem. Soc.* **2018**, *140*, 594−597.

(13) Jin, Y.; Zhang, C.; Dong, X.-Y.; Zang, S.-Q.; Mak, T. C. W. Shell engineering to achieve modification and assembly of atomically-precise silver clusters. *Chem. Soc. Rev.* **2021**, *50*, 2297−2319.

(14) Huang, R.-W.; Wei, Y.-S.; Dong, X.-Y.; Wu, X.-H.; Du, C.-X.; Zang, S.-Q.; Mak, T. C. W. Hypersensitive dual-function luminescence switching of a silver-chalcogenolate cluster-based metal−organic framework. *Nat. Chem.* **2017**, *9*, 689−697.

(15) Xie, Z.; Sun, P.; Wang, Z.; Li, H.; Yu, L.; Sun, D.; Chen, M.; Bi, Y.; Xin, X.; Hao, J. Metal−Organic Gels from Silver Nanoclusters with Aggregation-Induced Emission and Fluorescence-to-Phosphorescence Switching. *Angew. Chem., Int. Ed.* **2020**, *59*, 9922−9927.

(16) Liu, J.-W.; Feng, L.; Su, H.-F.; Wang, Z.; Zhao, Q.-Q.; Wang, X.-P.; Tung, C.-H.; Sun, D.; Zheng, L.-S. Anisotropic Assembly of Ag_{52} and Ag_{76} Nanoclusters. *J. Am. Chem. Soc.* **2018**, *140*, 1600−1603.

(17) Pei, X.-L.; Guan, Z.-J.; Nan, Z.-A.; Wang, Q.-M. Heterometallic Coinage Metal Acetylenediide Clusters Showing Tailored Thermochromic Luminescence. *Angew. Chem., Int. Ed.* **2021**, *60*, 14381−14384.

(18) Lei, Z.; Wan, X.-K.; Yuan, S.-F.; Guan, Z.-J.; Wang, Q.-M. Alkynyl Approach toward the Protection of Metal Nanoclusters. *Acc. Chem. Res.* **2018**, *51*, 2465−2474.

(19) Liu, W.-D.; Wang, J.-Q.; Yuan, S.-F.; Chen, X.; Wang, Q.-M. Chiral Superatomic Nanoclusters Ag_{47} Induced by the Ligation of Amino Acids. *Angew. Chem., Int. Ed.* **2021**, *60*, 11430−11435.

(20) Monticelli, M.; Baron, M.; Tubaro, C.; Bellemin-Laponnaz, S.; Graiff, C.; Bottaro, G.; Armelao, L.; Orian, L. Structural and Luminescent Properties of Homoleptic Silver(I), Gold(I), and Palladium(II) Complexes with *n*NHC-*tz*NHC Heteroditopic Carbene Ligands. *ACS Omega* **2019**, *4*, 4192−4205.

(21) Wang, Z.; Li, M.-D.; Shi, J.-Y.; Su, H.-F.; Liu, J.-W.; Feng, L.; Gao, Z.-Y.; Xue, Q.-W.; Tung, C.-H.; Sun, D. In Situ Capture of a Ternary Supramolecular Cluster in a 58-Nuclei Silver Supertetrahedron. *CCS Chem.* **2021**, *3*, 1873−1880.

(22) Rendošová, M.; Gyepes, R.; Maruščáková, I. C.; Mudroňová, D.; Sabolová, D.; Kello, M.; Vilková, M.; Almáši, M.; Huntošová, V.; Zemek, O.; Vargová, Z. An in vitro selective inhibitory effect of silver(I) aminoacidates against bacteria and intestinal cell lines and elucidation of the mechanism of action by means of DNA binding properties, DNA cleavage and cell cycle arrest. *Dalton Trans.* **2021**, *50*, 936−953.

(23) Nomiya, K.; Takahashi, S.; Noguchi, R.; Nemoto, S.; Takayama, T.; Oda, M. Synthesis and Characterization of Water-Soluble Silver(I) Complexes with *L*-Histidine (H_2his) and (*S*)-(−)-2-Pyrrolidone-5-carboxylic Acid (H_2pyrrld) Showing a Wide Spectrum of Effective Antibacterial and Antifungal Activities. Crystal Structures of Chiral Helical Polymers $[Ag(Hhis)]_n$ and $\{[Ag(Hpyrrld)]_2\}_n$ in the Solid State. *Inorg. Chem.* **2000**, *39*, 3301−3311.

(24) Kasuga, N. C.; Takagi, Y.; Tsuruta, S.-i.; Kuwana, W.; Yoshikawa, R.; Nomiya, K. Synthesis, structure and antimicrobial activities of meso silver(I) histidinate $[Ag_2(D\text{-his})(L\text{-his})]_n$ (Hhis=histidine) showing different self-assembly from those of chiral silver(I) histidinates. *Inorg. Chim. Acta* **2011**, *368*, 44−48.

(25) Nomiya, K.; Yokoyama, H. Syntheses, crystal structures and antimicrobial activities of polymeric silver(i) complexes with three amino-acids [aspartic acid (H_2asp), glycine (Hgly) and asparagine (Hasn)]. *J. Chem. Soc., Dalton Trans.* **2002**, 2483−2490.

(26) Chabert, V.; Hologne, M.; Sénèque, O.; Crochet, A.; Walker, O.; Fromm, K. M. Model peptide studies of Ag^+ binding sites from the silver resistance protein SilE. *Chem. Commun.* **2017**, *53*, 6105−6108.

(27) Eckhardt, S.; Brunetto, P. S.; Gagnon, J.; Priebe, M.; Giese, B.; Fromm, K. M. Nanobio Silver: Its Interactions with Peptides and Bacteria, and Its Uses in Medicine. *Chem. Rev.* **2013**, *113*, 4708−4754.

(28) Khan, S. A.; Reshak, A. H. Linear, nonlinear optical susceptibilities, hyperpolarizability, and space electronic charge density of meso silver(I) histidinate $[Ag(D\text{-his})]_n$ (Hhis=histidine). *Polyhedron* **2015**, *85*, 962−970.

(29) Mirolo, L.; Schmidt, T.; Eckhardt, S.; Meuwly, M.; Fromm, K. M. pH-Dependent Coordination of Ag^I Ions by Histidine: Experiment, Theory, and a Model for SilE. *Chem. − Eur. J.* **2013**, *19*, 1754−1761.

(30) Yan, Z.-H.; Li, X.-Y.; Liu, L.-W.; Yu, S.-Q.; Wang, X.-P.; Sun, D. Single-Crystal to Single-Crystal Phase Transition and Segmented Thermochromic Luminescence in a Dynamic 3D Interpenetrated AgI Coordination Network. *Inorg. Chem.* **2016**, *55*, 1096−1101.

(31) Wang, X.-P.; Chen, W.-M.; Qi, H.; Li, X.-Y.; Rajnák, C.; Feng, Z.-Y.; Kurmoo, M.; Boča, R.; Jia, C.-J.; Tung, C.-H.; Sun, D. Solvent-Controlled Phase Transition of a Co^{II}-Organic Framework: From Achiral to Chiral and Two to Three Dimensions. *Chem. − Eur. J.* **2017**, *23*, 7990−7996.

(32) Banti, C. N.; Raptopoulou, C. P.; Psycharis, V.; Hadjikakou, S. K. Novel silver glycinate conjugate with 3D polymeric intermolecular self-assembly architecture; an antiproliferative agent which induces apoptosis on human breast cancer cells. *J. Inorg. Biochem.* **2021**, *216*, No. 111351.

(33) Sheldrick, G. M. *SHELXT*-Integrated Space-Group and Crystal-Structure Determination. *Acta Crystallogr A Found Adv* **2015**, *71*, 3−8.

https://doi.org/10.1021/acsomega.2c00094
ACS Omega 2022, 7, 8141−8149

(34) Dolomanov, O. V.; Bourhis, L. J.; Gildea, R. J.; Howard, J. A.; Puschmann, H. OLEX2: a complete structure solution, refinement and analysis program. *J. Appl. Crystallogr.* **2009**, *42*, 339−341.
(35) Bondi, A. van der Waals Volumes and Radii. *J. Phys. Chem. A* **1964**, *68*, 441−451.
(36) Schmidbaur, H.; Schier, A. Argentophilic Interactions. *Angew. Chem., Int. Ed.* **2015**, *54*, 746−784.
(37) Pyykkö, P. Strong Closed-Shell Interactions in Inorganic Chemistry. *Chem. Rev.* **1997**, *97*, 597−636.
(38) Jin, J.; Wang, W.; Liu, Y.; Hou, H.; Fan, Y. A precise hexagonal octadecanuclear Ag macrocycle with significant luminescent properties. *Chem. Commun.* **2011**, *47*, 7461−7463.
(39) Li, B.; Huang, R.-W.; Qin, J.-H.; Zang, S.-Q.; Gao, G.-G.; Hou, H.-W.; Mak, T. C. W. Thermochromic Luminescent Nest-Like Silver Thiolate Cluster. *Chem. − Eur. J.* **2014**, *20*, 12416−12420.

https://doi.org/10.1021/acsomega.2c00094
ACS Omega 2022, 7, 8141−8149